

Journal of Materials Chemistry A

Accepted Manuscript



This is an *Accepted Manuscript*, which has been through the Royal Society of Chemistry peer review process and has been accepted for publication.

Accepted Manuscripts are published online shortly after acceptance, before technical editing, formatting and proof reading. Using this free service, authors can make their results available to the community, in citable form, before we publish the edited article. We will replace this *Accepted Manuscript* with the edited and formatted *Advance Article* as soon as it is available.

You can find more information about *Accepted Manuscripts* in the [Information for Authors](#).

Please note that technical editing may introduce minor changes to the text and/or graphics, which may alter content. The journal's standard [Terms & Conditions](#) and the [Ethical guidelines](#) still apply. In no event shall the Royal Society of Chemistry be held responsible for any errors or omissions in this *Accepted Manuscript* or any consequences arising from the use of any information it contains.

Vertically aligned graphene nanosheets on silicon using an ionic liquid electrolyte: Towards high performance on-chip micro-supercapacitors

David Aradilla,^{*a,b,c} Marc Delaunay,^{*d,e} Saïd Sadki,^{a,b,c} Jean-Michel Gérard^{d,e} and Gérard Bidan^{f,g}

^aUniv. Grenoble Alpes, INAC-SPRAM, F-38000 Grenoble, France

^bCNRS, SPRAM, F-38000 Grenoble, France

^cCEA, INAC-SPRAM, F-38000 Grenoble, France

^dUniv. Grenoble Alpes, INAC-SP2M, F-38000 Grenoble, France

^eCEA, INAC-SP2M, F-38000 Grenoble, France

^fUniv. Grenoble Alpes, INAC-DIR, F-38000 Grenoble, France

^gCEA, INAC-DIR, F-38000 Grenoble, France

*Corresponding authors: david.aradilla@cea.fr and marc.delaunay@cea.fr

Abstract

Vertically oriented graphene nanosheets were synthesized by an alternative and simple approach based on electron cyclotron resonance-plasma enhanced chemical vapor deposition (ECR-CVD) onto highly doped silicon substrates. The as-grown graphene electrodes were employed in a symmetric micro-supercapacitor using an aprotic ionic liquid [N-methyl-N-propylpyrrolidinium bis(trifluoromethylsulfonylimide; PYR₁₃TFSI)] as electrolyte. The device was able to deliver an outstanding specific capacitance value of 2 mF cm⁻², a power density value of 4 mW cm⁻² and an energy density value of 4 μWh cm⁻² operating at a large and stable cell voltage of 4V with a quasi-ideal capacitive behaviour. Moreover, the lifetime of the device exhibited a remarkable electrochemical stability retaining 80 % of the initial capacitance after 150000 galvanostatic charge-discharge cycles at a high current density of 1 mA cm⁻². This excellent electrochemical performance results from the obtained channel-based 3-D graphene network promoting rapid electrolyte ion-transport and short diffusion paths.

1. Introduction

Over the past years, the development of innovative technological applications in the field of micro and nanotechnology, such as micro-electronics, micro-medicine or nano-engineering, has sparked a great deal of attention in the research of high performance energy storage units. Within this context miniaturized electronic devices, as for example micro-electromechanical systems (MEMS), radiofrequency identification (RFID) tags, wireless sensor nodes, embedded micro-sensors or biomedical implants (e.g. neurotransmitters) require micro-power sources with small dimensions and high power densities.^{1,2} In this regard micro-supercapacitors (μ -SCs), also known as micro-ultracapacitors, have emerged as alternative and prospective electrochemical energy storage devices due to their interesting properties in terms of high power density and efficiency, fast charge and discharge rate, excellent reversibility, long lifespan and relative low cost, which make them attractive in a wide range of modern and smart industrial applications.³

Recently, tremendous efforts have been devoted to develop novel high-performance micro-supercapacitors based on nanostructured material electrodes with advanced architectures. From this perspective, new materials based on nanostructured silicon (e.g. silicon nanowires SiNWs,⁴⁻⁸ silicon nanotrees SiNTrs⁹ or silicon carbide nanowires SiCNWs),¹⁰⁻¹² transition metal carbides and carbonitrides (e.g. MXenes)¹³ or nanostructured carbonaceous materials as for example onion-like carbon,^{14,15} carbide derived carbon,¹⁶ or carbon nanotubes^{17,18} have attracted a special interest in the field of micro-supercapacitor devices owing to their unique properties in terms of long cyclability and high power pulse. In spite of the important progress and advancements carried out in this direction, the development of high performance micro-supercapacitors remains still a challenge. In order to achieve this goal, currently a special interest has been focused on graphene as an excellent two dimensional (2D) nanostructured material. Graphene is an attractive and robust material to be employed as micro-supercapacitor electrode due to its exceptional in-plane electrical conductivity (up to 20 000 S cm⁻¹), high surface-to-volume ratio, large surface area (2630 m² g⁻¹) and high thermal conductivity (\sim 5300 W m⁻¹ K⁻¹).¹⁹ In addition, graphene has shown a remarkable theoretical capacitance of 550 F g⁻¹.²⁰ Accordingly, in recent years micro-supercapacitors based on graphene electrodes have been extensively investigated, demonstrating their high capabilities in terms of high power and energy densities.^{21,22}

Nowadays, graphene has been synthesized mainly through several methods based on exfoliation, epitaxial growth, graphene oxide reduction and chemical vapor deposition

approaches.²³ Among various plasma based techniques (dc plasma discharge, ICP-plasma or thermal plasma jet system), the plasma enhanced chemical vapor deposition (PECVD) technique has been demonstrated to be an excellent strategy for the synthesis of vertically oriented graphene, which provides high conductance channels and efficient ion transport for access and escape of the electrolyte between the nanosheets. This characteristic has been demonstrated to play a crucial role on the enhancement of the capacitive properties of micro-supercapacitors.²⁴ Thus, micro-supercapacitors based on vertical graphene nanosheets (VGNs) grown by PECVD have been evaluated using different metallic substrates (e.g. nickel or copper) with excellent capacitive properties in presence of aqueous solvents containing potassium hydroxide (KOH) as electrolyte.²⁵⁻²⁸ As a consequence, these micro-devices have showed very interesting results in terms of specific capacitance ($265 \mu\text{F cm}^{-2}$).^{25,27} Nevertheless, scarce works have been reported dealing with the deposition of vertically oriented graphene by chemical vapor deposition approaches for micro-supercapacitor applications. Presently, most of them have been focused on PECVD and RFCVD techniques.²⁵⁻³¹

In this work, we report the synthesis and application of VGNs deposited on highly doped silicon substrates through an alternative and catalyst-free method based on electron cyclotron resonance-plasma enhanced chemical vapor deposition (ECR-CVD) technique. The graphene-based electrodes were employed in a symmetric micro-supercapacitor device using an aprotic ionic liquid (PYR₁₃TFSI) as electrolyte, which was used owing to its moderate viscosity (47 cP at 20°C) and wide voltage stability window (4V).^{8,32} Subsequently, a complete and detailed electrochemical characterization of the micro-device was evaluated by cyclic voltammetry (CV), galvanostatic charge-discharge cycles and electrochemical impedance spectroscopy (EIS) respectively. Furthermore, an exhaustive morphological and structural characterization of the graphene electrodes was carried out by using scanning electron microscopy, transmission electron microscopy and Raman spectroscopy.

2. Experimental section

Materials. Highly n-doped Si (111) substrates (doping level: $5 \cdot 10^{18}$ doping atoms cm^{-3}) and resistivity less than $0.005 \Omega \text{ cm}$ were used as the substrate for VGNs growth. N-methyl-N-propylpyrrolidinium bis(trifluoromethylsulfonyl)imide was purchased from IOLITEC (Ionic Liquids Technologies GmbH, Germany) and used without further purification.

Description of the ECR-CVD reactor. The ECR plasma source, built in our Institute, was described previously.^{33,34} Briefly, The ECR-CVD reactor consists of a 2.45 GHz microwave power injection, two permanent magnets providing the required magnetic field for electron resonance and plasma confinement, a gas inlet and a substrate heater (Figure 1a).

Synthesis of vertical graphene nanosheets (VGNs) on silicon substrates. Prior to the VGNs growth, Si wafer surface (1 cm^2) was cleaned by successive dipping in acetone, isopropanol and Caro ($\text{H}_2\text{SO}_4:\text{H}_2\text{O}_2$, 3:1 v/v) solutions in order to remove organic impurities. After that, the substrates were dipped in 10% HF and NH_4F solution to remove the native oxide layer. Subsequently, Si(111) substrate was loaded into the growth chamber and the chamber was pumped down to $2 \cdot 10^{-3}$ mbar. At a sample holder temperature of 500°C the substrate was etched by H_2 plasma during 6 min at a microwave power of 250 W. After this pre-cleaning step, 50 sccm C_2H_4 gas flow was injected into the chamber at a temperature of 620°C using a microwave power of 280 W. The synthesis growth was varied from 0.2 to 4 h respectively. The growth mechanism of vertically graphene nanosheets is based on the dissociation and ionization of ethylene achieved step-by-step by electron impact in order to create carbon radicals and ions (Figure 1b). The trajectories of the produced ions and electrons are guided by the magnetic field lines in the plasma chamber. The substrate is located in the plasma chamber, on the axis of the static magnetic field.

Morphological and structural characterization of the electrodes. The morphology of VGNs electrodes was characterized using a Zeiss Ultra 55 electron microscope at an accelerating voltage of 4 kV and a JEOL 3010 transmission electron microscopy at an accelerating voltage of 300 kV. Raman spectra measurement was conducted on a WITEC Alpha 500 spectrometer with a 532 nm laser excitation, a laser power of 1 mW and a spot diameter of 400 nm.

Design of the micro-supercapacitor. The symmetric micro-supercapacitor was designed using a homemade 2-electrode elementary cell in a planar configuration. The micro-supercapacitor device was built by assembling two VGNs-based nanostructured electrodes

separated by a Whatman glass fiber paper separator soaked with the electrolyte (PYR₁₃TFSI). The nanostructured sides (graphene nanosheets) are in contact with the separator soaked by the electrolyte and the others are in contact with a stainless steel current collector.

Electrochemical characterization of the micro-supercapacitor. The performance of the micro-supercapacitor device was evaluated using cyclic voltammetry (CV), galvanostatic charge-discharge cycles and electrochemical impedance spectroscopy (EIS). All measurements were performed in an argon filled glove box with oxygen and water levels less than 1 ppm at room temperature using a multichannel VMP3 potentiostat/galvanostat with Ec-Lab software (Biologic, France). CV curves were measured at different scan rates from 0.2 to 30 Vs⁻¹ and galvanostatic charge-discharge cycle measurements were conducted under various current densities from 0.25 to 2 mA cm⁻² between 0 and 4 V. EIS tests were performed using a frequency range between 400 kHz to 10 mHz with ac perturbation of 10 mV.

3. Results and discussion

The morphology of VGNs was characterized by SEM and TEM as illustrated in Figure 2. Figure 2a and 2b show the top-view SEM micrographs of VGNs deposited onto highly doped substrates using a deposition time of 40 min. As can be seen, the cross sectional views reflect a 2- μm thickness coating. According to the figures 2a and 2b, it can be clearly observed that graphene-like structure was deposited perpendicularly with respect to the surface of the substrate keeping a uniform, dense, and porous network. A more detailed characterization of the graphene nanosheets was performed by TEM. Figure 2c shows a high-resolution TEM image of the typical sheet edges grown at the temperature of 620°C during 40 min. The graphene sheets show sharp and transparent edges and their thickness was determined to be around 1 nm. The graphene nanosheet growth rate was estimated from the film thickness using the cross sectional of samples. Thus, the results depicted in Figure 2d reflect a linear dependence of the thickness of the graphene film as a function of the deposition time. The growth rate was measured to be about 2.85 $\mu\text{m h}^{-1}$ from a linear regression fit of the plot displayed in Figure 2d.

Raman spectroscopy was employed to confirm the structure of VGNs grown by ECR-CVD. Figure 3 shows the corresponding Raman spectrum where two characteristic bands were detected, G ($\sim 1580 \text{ cm}^{-1}$) and 2D ($\sim 2700 \text{ cm}^{-1}$) respectively. These bands are indicative of a graphitic structure.³⁵ The presence of the D peak ($\sim 1358 \text{ cm}^{-1}$) is associated with local defects into the structure, which are attributed to edge chirality, disorder or breakdown of translational symmetry.³⁶ Another important characteristic concerning the quality of graphene is related with the I_D / I_G ratio. In this particular case, the I_D / I_G intensity ratio was calculated to be approximately 1.50, which suggests that the material possesses a low defect level according to previous works reported in the literature.^{37,38} Thus, this value was found to be in excellent agreement. In parallel, other two significant peaks were identified with one and two phonon defect-assisted processes denoted as D and D+D'.³⁹ Although the intensity of defects found in the material is relatively important, the results confirm the success of graphene growth on silicon substrates by ECR-CVD technique. Figure 4a shows the CV curves recorded at a scan rate of 20 V s^{-1} for the graphene-based symmetric micro-supercapacitors using graphene deposition times of 0.2, 0.4, 2 and 4h respectively. As can be seen, all the CV curves exhibit a nearly rectangular shape with a perfect mirror-image feature indicating the excellent capacitive behavior of the device in the potential range from 0 to 4 V. This feature demonstrates also a quasi-pure electrochemical double layer capacitor. It is worth to mention

that GNs deposited at a total time of 4h show the highest capacitance due to their higher surface area, which provides better conductive paths for the ions mobility during the adsorption-desorption processes. This tendency was corroborated in Figure 4b showing the evolution of the CV curves at different scan rates ranged from 1 to 30 Vs^{-1} . As it can be observed, the CV responses exhibit an excellent capacitive behavior with quasi-rectangular loops even at very high scan rates ($> 20 \text{Vs}^{-1}$), demonstrating its high charge-discharge capability rate. Within this context, galvanostatic charge-discharge measurements were also tested with a nearly triangular shape and linear slopes as displayed in Figure 4c. The profiles indicate an excellent electrochemical capacitive characteristic and high reversibility between charge and discharge processes at a current density of 0.25mA cm^{-2} for all the micro-supercapacitors. The charge-discharge cycles are similar in shape between 0 and 4 V demonstrating that the micro-supercapacitors can be stably performed in a wide cell voltage. Accordingly, at a high current density of 1mA cm^{-2} this tendency was corroborated as illustrated in Figure 4d. The specific capacitance (SC) of the micro-devices was calculated from the discharge curves at different current densities ($0.25 - 2 \text{mA cm}^{-2}$) using the following equation:

$$SC = \frac{I \Delta t}{\Delta V A} \quad (1)$$

where SC (mF cm^{-2}) is the specific capacitance of the micro-supercapacitor, I (mA) corresponds to the discharge current, ΔV (V) is the potential change within the discharge time Δt (s), and A (cm^2) refers to the area of the electrodes. The calculated specific capacitance as a function of the discharge current is plotted in Figure 4e. As it was mentioned previously, the highest specific capacitance values were found when graphene was grown on the electrodes at a deposition time of 4h (Thickness: $12 \mu\text{m}$). Specifically, a specific capacitance value of $\sim 2 \text{mF cm}^{-2}$ was obtained at a high current density of 2mA cm^{-2} . This value was found higher than findings reported previously in the literature. Within this context, other electrochemical double layer micro-supercapacitors based on CVD-grown nanostructured electrodes exhibited lower SC values as for example SiNWs (SC: $23 - 50 \mu\text{F cm}^{-2}$),^{4,5,8} SiNTrs (SC: $84 \mu\text{F cm}^{-2}$)⁹ or carbon nanotubes (SC: $430 \mu\text{F cm}^{-2}$ and 1mF cm^{-2}).^{18,40} From this perspective, recently interdigitated on-chip micro-supercapacitors based on nanostructured carbon material electrodes such as carbide derived carbon films,¹⁶ onion-like carbon,¹⁵ graphene⁴¹ or multi-walled carbon nanotubes⁴² exhibited specific capacitance values ranging from 1 up to 3mF cm^{-2} . More specifically, regarding micro-supercapacitors based on graphene electrodes

obtained by chemical reduction of the graphene oxide (rGO) the values reported in the literature were ranged from 0.50 up to 1.8 mF cm⁻².²¹ Consequently, the values represented in this work reflect that VGNs electrodes grown by ECR-CVD are a promising alternative to be employed in energy storage electrochemical devices, particularly in the field of μ -SCs. Again, VGNs with a thickness of 12 μ m show the highest specific capacitance, which indicates that morphology and surface of graphene play an important role on the capacitive and electrochemical properties of micro-supercapacitors. This improvement is attributed to the highly porous structure, high surface area and shortened diffusion paths which favour ion transfer in the electrode-electrolyte interface and faster kinetics. For a better comprehension of this matter, figure 4f shows the Nyquist plot of the micro-supercapacitor device in the frequency ranging from 400 kHz to 10 mHz. The plot shows a straight line in the low frequency region, a depressed semicircle in the high-to-medium frequency region and a high frequency intercepts in the real Z axis. At high frequency, the intercept of the curve with the real axis indicates the equivalent series resistance (ESR), which represents the sum of the ionic resistance of the electrolyte, the intrinsic resistance of the active materials and the contact resistance at the active material/current collector interface. A ESR value of 24 Ω cm⁻² was calculated according to the inset displayed in Figure 4f, which leads a maximal power density (P^{\max} : $V^2/4ESR$) of 167 mW cm⁻². This value was found in excellent agreement with other carbon-based micro-supercapacitors performed on silicon substrates. Thus, P^{\max} values of 34 mW cm⁻² or 240 mW cm⁻² were estimated in previous studies.^{43,15} The semicircle in the high-to-medium frequency region represents the charge transfer resistance (R_{ct}) with a value of $\sim 7 \Omega$ cm². This region was ascribed to the silicon oxidation layer formed on the substrate according to our previous work.⁴⁴ The straight line in the low frequency region corresponds to the ion diffusion-controlled region, where a capacitive behavior is represented (e.g. the more vertical line is indicative of an electrode more close to an ideal capacitor). Additionally, the EIS technique is also a powerful tool in order to evaluate the capacitive behavior of a micro-supercapacitor. Thus, the imaginary part of the complex capacitance versus frequency can be obtained according to the following equation:⁴⁵

$$C''(\omega) = \frac{Z'(\omega)}{\omega|Z(\omega)|^2} \quad (2)$$

where $C''(\omega)$ is the imaginary part of the capacitance, $Z(\omega)$ is the impedance, $Z'(\omega)$ is the real part of the impedance and $\omega=2\pi f$ where f corresponds to the frequency. The $C''(\omega)$ corresponds to an energy dissipation by an irreversible process that can lead to a hysteresis.⁴⁵

Figure 5a shows the evolution of C'' versus frequency for the SiNWs micro-supercapacitor. This plot allows to evaluate an important property on the performance of micro-supercapacitors related with the relaxation time constant of the device (τ_0). This parameter is defined as the minimum time needed to discharge all the energy from the device with an efficiency of more than 50%.¹⁴ From the plot displayed in Figure 5a, the time constant was evaluated using the following relation ($\tau_0=1/f_0$), which was calculated to be 290 ms. This value was found lower than other micro-supercapacitors reported in the literature based on carbon electrodes as for example activated carbon ($\tau_0=700$ ms).¹⁴ Therefore, VGNs electrodes in presence of $\text{PYR}_{13}\text{TFSI}$ as electrolyte possess a great potential for the instantaneous delivery of high power. Figure 5b illustrates the impedance phase angle dependence on frequency (Bode plot). As can be observed, at frequencies lower than 330 Hz the phase angle of the micro-supercapacitor corresponds to $\sim 84^\circ$, close to 90° for ideal capacitor. The specific capacitance value at 120 Hz, frequency typically required for alternating current line filtering applications, was calculated using the following formula:

$$\text{SC} = \frac{-1}{2\pi f Z''} \quad (3)$$

A SC value of 0.27 mF was obtained from the figure 5b. This value was found in excellent agreement compared with others micro-supercapacitors based on vertically oriented graphene electrodes (SC: 0.2 - 0.4 mF).^{26,46} From the Bode plot, the frequency at which the phase angle crosses 45° is described also as an important feature to determine the frequency response of a micro-supercapacitor, thus higher frequency implies faster device switching.¹⁸ Regarding the state of the art commercial EDLCs based on activated carbon electrode materials, they present a 45° phase angle at ~ 0.2 Hz.⁴⁶ In this study, the micro-supercapacitors based on VGNs electrodes show a 45° phase angle at ~ 3 Hz, indicating a very fast frequency response and excellent capacitive behaviour.

Power and energy densities are also two key performance indicators for evaluating the applications of micro-supercapacitor devices. Figure 6a shows the Ragone plot used to determine the energy density (E , $\mu\text{Wh cm}^{-2}$) and power density (P , $\mu\text{W cm}^{-2}$) of VGNs-based micro-supercapacitors according to the following equations:

$$E = \frac{1}{2} \text{SC} \Delta V^2 \quad (4)$$

$$P = \frac{E}{\Delta t} \quad (5)$$

Particularly, the Ragone plot increases rapidly with power density due to the fast voltage decay during discharge as shown in Figure 6a. The micro-supercapacitor devices exhibit energy and power density values ranging from $4 \mu\text{Wh cm}^{-2}$ up to $4.5 \mu\text{Wh cm}^{-2}$ and from 0.5 up to 4 mW cm^{-2} using wide current densities (e.g. $0.25 - 2 \text{ mA cm}^{-2}$). These values were compared with those obtained in our previous studies dealing with CVD grown-SiNWs. Here, the results obtained in this investigation indicate an extraordinary enhancement of the electrochemical performance in terms of power and energy densities over EDL micro-supercapacitors based on nanostructured silicon, which exhibit a typical energy density of $0.05 - 0.27 \mu\text{Wh cm}^{-2}$ and a power density of $0.1 - 2 \text{ mW cm}^{-2}$.^{8,9,47} In addition, the obtained volumetric energy and power densities represented in Figure 6b were also compared with other graphene-based micro-supercapacitor demonstrating again the potential of VGNs for micro-supercapacitor applications. Thus, a volumetric power density of 5 W cm^{-3} was calculated for our system, which exhibit better performance than rGO based-micro-supercapacitors (1.7 W cm^{-3})⁴⁸ or rGO/CNT micro-supercapacitors (2.5 W cm^{-3}).⁴¹ Regarding the volumetric energy density a value of 5 mWh cm^{-3} was calculated. This value was found to be higher than micro-supercapacitors based on rGO. Thus, values of 0.23 mWh cm^{-3} , 2.7 mWh cm^{-3} , 0.43 mWh cm^{-3} or 0.3 mWh cm^{-3} were recently reported in the literature.^{49, 41, 48, 50}

Cycling stability is another important key indicator on the performance of micro-supercapacitors. Long cycle life test has been performed for the symmetric VGNs micro-supercapacitors applying successive galvanostatic charge-discharge cycles at a current density of 1 mA cm^{-2} over 150000 cycles between 0 and 4 V. The normalized capacitance as a function of cycle-number is reflected in Figure 7a. The devices show an excellent electrochemical stability, after cycling 150000 times the devices experience indeed less than 20% reduction of its initial capacitance value. Similar values were obtained for the micro-supercapacitor devices based on VGNs electrodes at different deposition times (0.2, 0.4 and 2h and 4h respectively). The lifetime of the devices was found higher than other micro-supercapacitors based on graphene materials as for example rGO, which showed a loss of $\sim 30\%$ after 10000 galvanostatic cycles.⁴⁸

On the other hand, an excellent coulombic efficiency (η) defined as the ratio between the discharge and charge times was observed during the cycling, with a value of $\sim 99\%$ showing the complete reversibility of charge storage based on electrical double layer capacitance as displayed in Figure 7b. The morphology of the VGNs electrodes after cycling was examined by using SEM images as shown in the Figure 7c. As can be seen, the structure of VGNs was remained unchanged even after thousands of successive charge-discharge

cycles. This morphology was comparable to those observed in Figure 1a and 1b corresponding to VGNs as grown (e.g. not cycled in an electrochemical device).

4. Conclusions

In summary, we have demonstrated successfully the synthesis of vertically oriented graphene nanosheet electrodes to be employed in a micro-supercapacitor application using an alternative chemical vapor deposition approach based on ECR-CVD technique. The graphene nanosheets demonstrated easy and fast ion transport, short diffusion paths, large electroactive surface area, fast high frequency response and an extraordinary structural stability upon electrochemical cycling in a wide cell voltage of 4 V. As a result, the fabricated device showed an excellent electrochemical performance in terms of specific capacitance (2 mF cm^{-2}), energy ($4 \text{ } \mu\text{Wh cm}^{-2}$) and power (4 mW cm^{-2}) densities. The results reported in this work were found clearly enhanced compared with other micro-supercapacitors based on CVD-grown nanostructured silicon or carbon derivative electrodes. Consequently, ECR-CVD grown-graphene micro-supercapacitors open up a new era for the development of high performance on-chip energy storage micro-units for their integration into miniaturized electronic devices.

Acknowledgements

The authors thank Dr. Merijn Bronsgeest for the Raman analysis. The authors are also indebted to Dr. Jan Wimberg and Dr. Thomas J. S. Schubert (IOLITEC GmbH) for providing us the ionic liquid. This work has been performed with the use of the Hybriden facility at CEA-Grenoble (France).

References

- 1 T. Brousse, *Electrochemistry*, 2013, **81**, 773.
- 2 C. Meng, J. Maeng, S. W. M. John and P. P. Irazoqui, *Adv. Energy Mater.*, 2014, **4**, 1301269.
- 3 M. Beidaghi and Y. Gogotsi, *Energy Environ. Sci.*, 2014, **7**, 867.
- 4 F. Thissandier, A. Le Comte, O. Crosnier, P. Gentile, G. Bidan, E. Hadji, T. Brousse and S. Sadki, *Electrochem. Commun.*, 2012, **25**, 109.
- 5 F. Thissandier, N. Pauc, T. Brousse, P. Gentile and S. Sadki, *Nanoscale Research Lett.*, 2013, **8**, 38.
- 6 F. Thissandier, L. Dupré, P. Gentile, T. Brousse, G. Bidan, D. Buttard and S. Sadki, *Electrochim. Acta*, 2014, **117**, 159.
- 7 J. P. Alper, S. Wang, F. Rossi, G. Salvati, N. Yiu, C. Carraro and R. Maboudian, *Nano Lett.*, 2014, **14**, 1843.
- 8 D. Aradilla, P. Gentile, G. Bidan, V. Ruiz, P. Gomez-Romero, T. J. S. Schubert, H. Sahin, E. Frackowiak and S. Sadki, *Nano Energy*, 2014, **9**, 273.
- 9 F. Thissandier, P. Gentile, T. Brousse, G. Bidan and S. Sadki, *J. Power Sources*, 2014, **269**, 740.
- 10 L. Gu, Y. Wang, Y. Fang, R. Lu and J. Sha, *J. Power Sources*, 2013, **243**, 648.
- 11 J. P. Alper, M. S. Kim, M. Vincent, B. Hsia, V. Radmilovic, C. Carraro and R. Maboudian, *J. Power Sources*, 2013, **230**, 298.
- 12 J. P. Alper, A. Gutes, C. Carraro and R. Maboudian, *Nanoscale*, 2013, **5**, 4114.
- 13 M. Naguib, V. N. Mochalin, M. W. Barsoum and Y. Gogotsi, *Adv. Mater.*, 2014, **26**, 992.
- 14 D. Pech, M. Brunet, H. Durou, P. Huang, V. Mochalin, Y. Gogotsi, P. L. Taberna and P. Simon, *Nat. Nanotech.*, 2010, **5**, 651.
- 15 P. Huang, D. Pech, R. Lin, J. K. McDonough, M. Brunet, P. L. Taberna, Y. Gogotsi and P. Simon, *Electrochem. Commun.*, 2013, **36**, 53.
- 16 P. Huang, M. Heon, D. Pech, M. Brunet, P. L. Taberna, Y. Gogotsi, S. Lofland, J. D. Hettinger and P. Simon, *J. Power Sources*, 2013, **225**, 240.
- 17 T. M. Dinh, K. Armstrong, D. Guay and D. Pech, *J. Mater. Chem. A*, 2014, **2**, 7170.
- 18 B. Hsia, J. Marschewski, S. Wang, J. B. In, C. Carraro, D. Poulidakos, C. P. Grigoropoulos and R. Maboudian, *Nanotechnology*, 2014, **25**, 055401.
- 19 D. Wei and J. Kivioja, *Nanoscale*, 2013, **5**, 10108.

- 20 Z.-S. Wu, K. Parvez, X. Feng and K. Müllen, *Nat. Commun.*, 2013, **4**, 2487.
- 21 G. Xiong, C. Meng, R. G. Reifengerger, P. P. Irazoqui and T. S. Fisher, *Electroanalysis*, 2014, **26**, 30.
- 22 Z.-S. Wu, X. Feng and H-M. Cheng, *National Science Review*, 2014, **1**, 1.
- 23 P. Avouris and C. Dimitrakopoulos, *Materials Today*, 2012, **15**, 86.
- 24 J. Zhu, D. Yang, Z. Yin, Q. Yan and H. Zhang, *Small*, 2014, **10**, 3480.
- 25 M. Cai, R. A. Outlaw, R. A. Quinlan, D. Premathilake, S. M. Butler and J. R. Miller, *ACS Nano*, 2014, **8**, 5873.
- 26 G. Ren, X. Pan, S. Bayne and Z. Fan, *Carbon*, 2014, **71**, 94.
- 27 M. Cai, R. A. Outlaw, S. M. Butler and J. R. Miller, *Carbon*, 2012, **50**, 5481.
- 28 Z. Bo, Z. Wen, H. Kim, G. Lu, K. Yu and J. Chen, *Carbon*, 2012, **50**, 4379.
- 29 X. Wang, J. Liu, Y. Wang, C. Zhao and W. Zheng, *Mater. Research Bullet.*, 2014, **52**, 89.
- 30 J. R. Miller, R. A. Outlaw and B. C. Holloway, *Science*, 2010, **329**, 1637.
- 31 J. R. Miller, R. A. Outlaw and B. C. Holloway, *Electrochim. Acta*, 2011, **56**, 10443.
- 32 V. Ruiz, T. Huynh, S. R. Sivakkumar and A. G. Pandolfo, *RSC Adv.*, 2012, **2**, 5591.
- 33 M. Delaunay, Permanent magnet linear microwave plasma source. US6319372 B1 (1987).
- 34 M. Delaunay and E. Touchais, *Rev. Sci. Instrum.*, 1998, **69**, 2320.
- 35 Y. Hao, Y. Wang, L. Wang, Z. Ni, Z. Wang, R. Wang, C. K. Koo, Z. Shen and J. T. L. Thong, *Small*, 2010, **6**, 195.
- 36 J. K. Kim, E. J. D. Castro, Y. G. Hwang and C. H. Lee, *J. Korean Phys. Soc.*, 2011, **58**, 53.
- 37 Z. Bo, Y. Yang, J. Chen, K. Yu, J. Yan and K. Cen, *Nanoscale*, 2013, **5**, 5180.
- 38 J. Fang, I. Levchenko, S. Kumar, D. Seo, K. Ostriko, *Sci. Technol. Adv. Mater.* 2014, **15**, 055009.
- 39 A. C. Ferrari and D. M. Basko, *Nat. Nanotech.*, 2013, **8**, 235.
- 40 M. G. Hahm, A. L. M. Reddy, D. P. Cole, M. Rivera, J. A. Vento, J. Nam, H. Y. Jung, Y. L. Kim, N. T. Narayanan, D. P. Hashim, C. Galande, Y. J. Jung, M. Bundy, S. Karna, P. M. Ajayan and R. Vajtai, *Nano Lett.*, 2012, **12**, 5616.
- 41 M. Beidaghi and C. Wang, *Adv. Funct. Mater.*, 2012, **22**, 4501.
- 42 T. Mai Dinh, K. Armstrong, D. Guayc and D. Pech, *J. Mater. Chem. A*, 2014, **2**, 7170.
- 43 H. Drouot, D. Pech, D. Colin, P. Simon, P.-L. Taberna and M. Brunet, *Microsyst. Technol.*, 2012, **18**, 467.

- 44 N. Berton, M. Brachet, F. Thissandier, J. Le Bideau, P. Gentile, G. Bidan, T. Brousse and S. Sadki, *Electrochem. Commun.*, 2014, **41**, 31.
- 45 P. L. Taberna, P. Simon and J. F. Fauvarque, *J. Electrochem. Soc.*, 2003, **150**, A292.
- 46 J. R. Miller and R. A. Outlaw, *J. Electrochem. Soc.*, 2015, **162**, A5077.
- 47 F. Gao, G.-L. Lewes-Malandrakis, M. T. Wolfer, W. Müller-Sebert, P. Gentile, D. Aradilla, T. Schubert and C. E. Nebel, *Diamond and related Mater.*, 2015, **51**, 1.
- 48 W. Gao, N. Singh, L. Song, Z. Liu, A. L. Reddy, L. J. Ci, R. Vajtai, Q. Zhang, B. Q. Wei and P. M. Ajayan, *Nat. Nanotechnol.* 2011, **6**, 496.
- 49 M. El-Kady, V. Strong, S. Dubin and R. Kaner, *Science* 2012, **335**, 1326.
- 50 M. F. El-Kady and R. B. Kaner, *Nat. Commun.*, 2013, **4**, 1475.

Captions to Figures

Figure 1. a) Schematic of ECR-CVD equipment employed to synthesize the vertical graphene nanosheet electrodes. b) Reaction mechanisms associated with the vertical graphene nanosheet growth on highly doped silicon substrates.

Figure 2. a) and b) Low and high magnification SEM images of the cross sectional view of VGNs deposited using a deposition time of 4h on silicon substrates. c) TEM image of VGNs. d) Plot of VGNs film thickness vs growth time at a substrate temperature of 620°C.

Figure 3. Typical Raman spectroscopy of VGNs grown on Si substrates (blue line) and Si substrate (red line). The Raman spectra indicates graphene-type structures associated with the D, G, 2D, D' and D + D' bands respectively.

Figure 4. Electrochemical characterization of VGNs micro-supercapacitors. a) Cyclic voltammograms at a scan rate of 20 Vs⁻¹ using different deposition times of GNs at 0.2h (red line) 0.4h (green line), 2h (orange line) and 4h (blue line). b) Cyclic voltammograms of VGNs employing a deposition time of 4h at different scan rates (1, 5, 10, 20 and 30 Vs⁻¹ respectively). Arrow indicates the increase of scan rate. c) Galvanostatic charge-discharge cycles at a current density of 0.25 mA cm⁻² using different thickness of VGNs (1, 2, 6 and 12 μm respectively). d) The first six galvanostatic charge - discharge cycles at a current density of 1 mA cm⁻² between 0 and 4 V using a graphene thickness of 12 μm. e) Specific capacitance as a function of current densities (0.25 - 2 mA cm⁻²) at different thickness of 1 μm (red circle), 2 μm (green triangle), 6 μm (orange square) and 12 μm (blue diamond). f) Nyquist plot measured at 0 V after the conditions described in b). The impedances were measured using a frequency range from 400 kHz to 10 mHz. Inset shows magnified high frequency region.

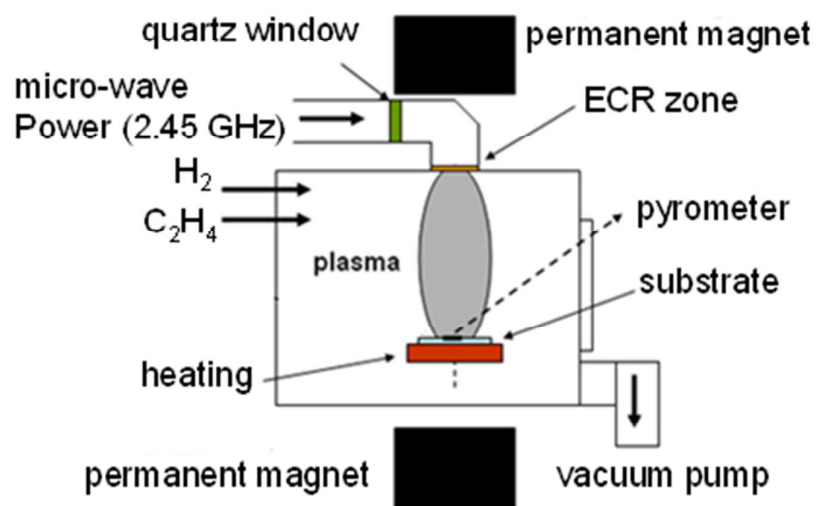
Figure 5. a) Evolution of the imaginary capacitance versus frequency for VGN micro-supercapacitor. The relaxation time constant (τ_0) of the device is indicated in the plot using an arrow. b) Bode plot of the micro-supercapacitor. The experimental conditions were adapted from figure 4f.

Figure 6. a) The Ragone plot per area for VGN (12 μm) micro-supercapacitors calculated by varying the discharging current density (0.25, 0.50, 0.75, 1 and to 2 mA

cm⁻² respectively). b) Plot of volumetric power and energy densities of VGN micro-supercapacitors using the same experimental conditions described in a).

Figure 7. Electrochemical stability of VGN based - micro-supercapacitors. a) Lifetime testing of the devices performed using 150000 complete charge-discharge cycles at a current density of 1 mA cm⁻² between 0 and 4 V. b) Coulombic efficiency as a function of number of galvanostatic cycles for a VGN (12 μm) microsupercapacitor. c) SEM micrograph of VGNs (12 μm) after cycling under the conditions described in a) at 45° tilted angle. VGNs were rinsed with acetone and isopropanol to ensure removal of excess electrolyte after electrochemical testing.

a)



b)

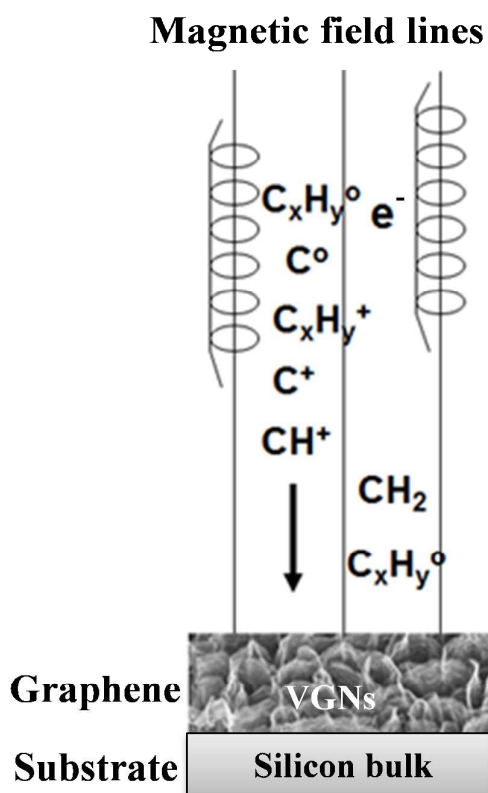


Figure 1

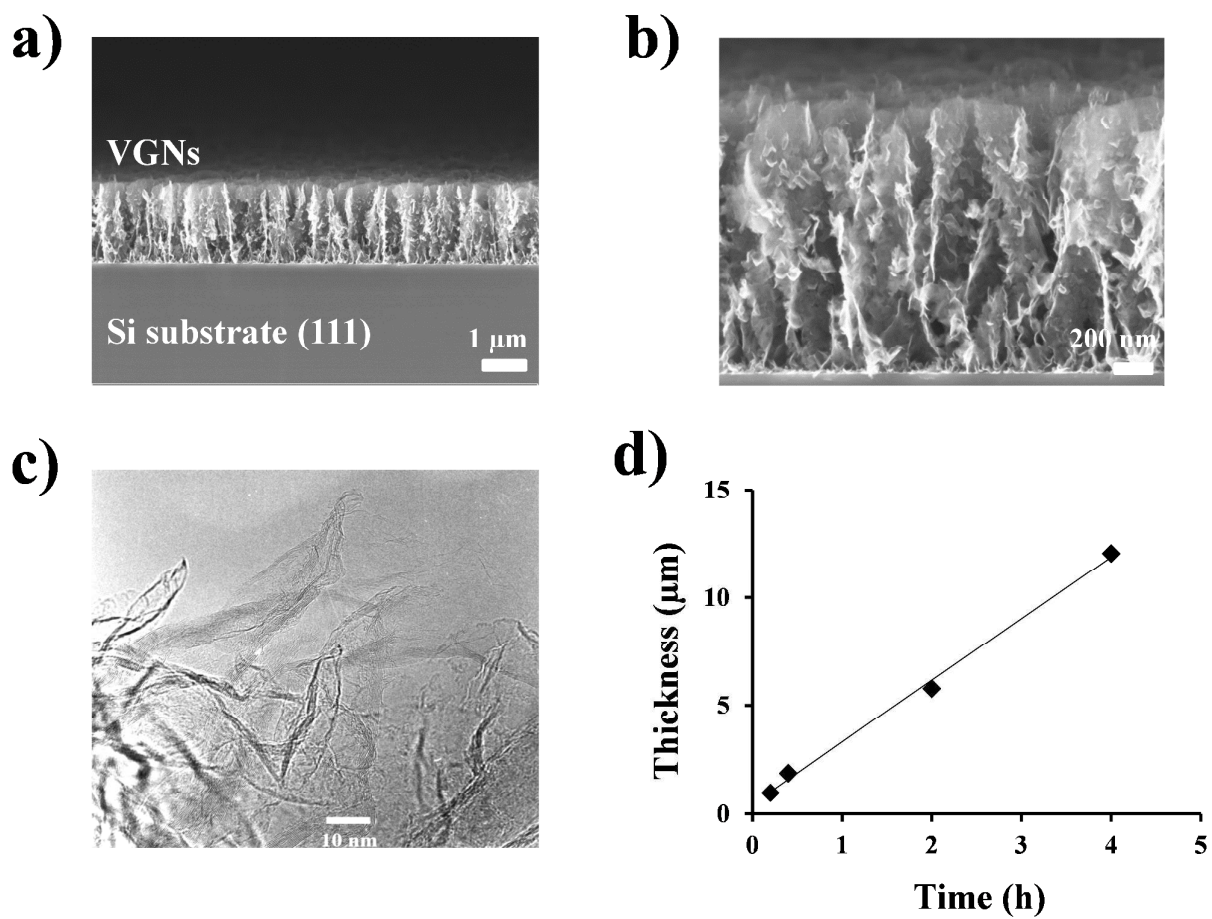
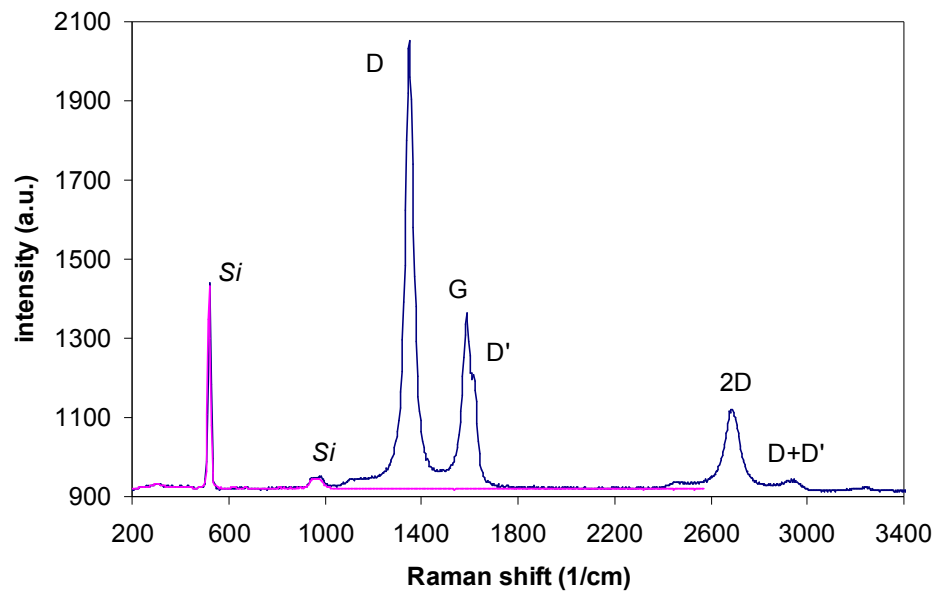


Figure 2

**Figure 3**

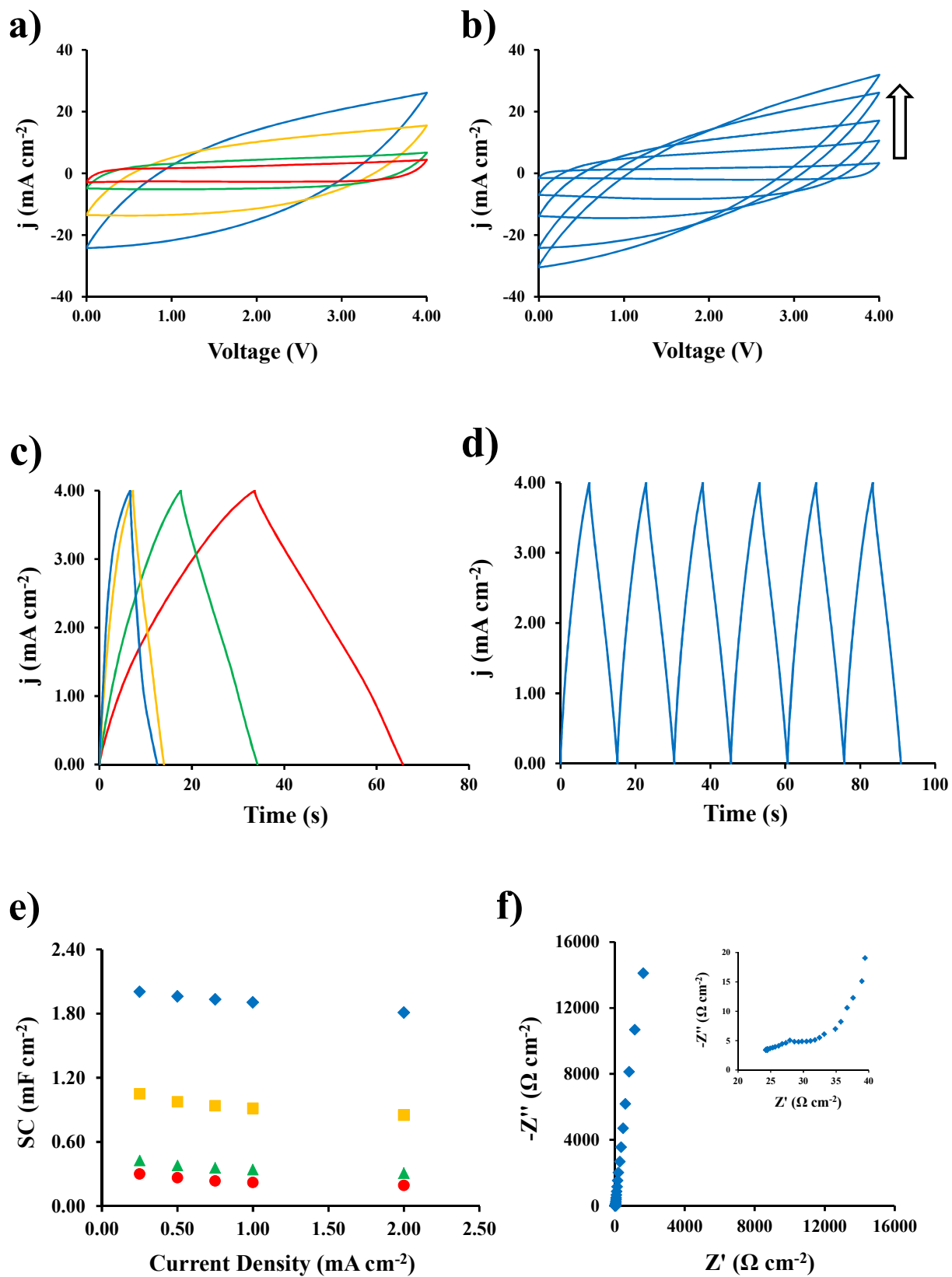


Figure 4

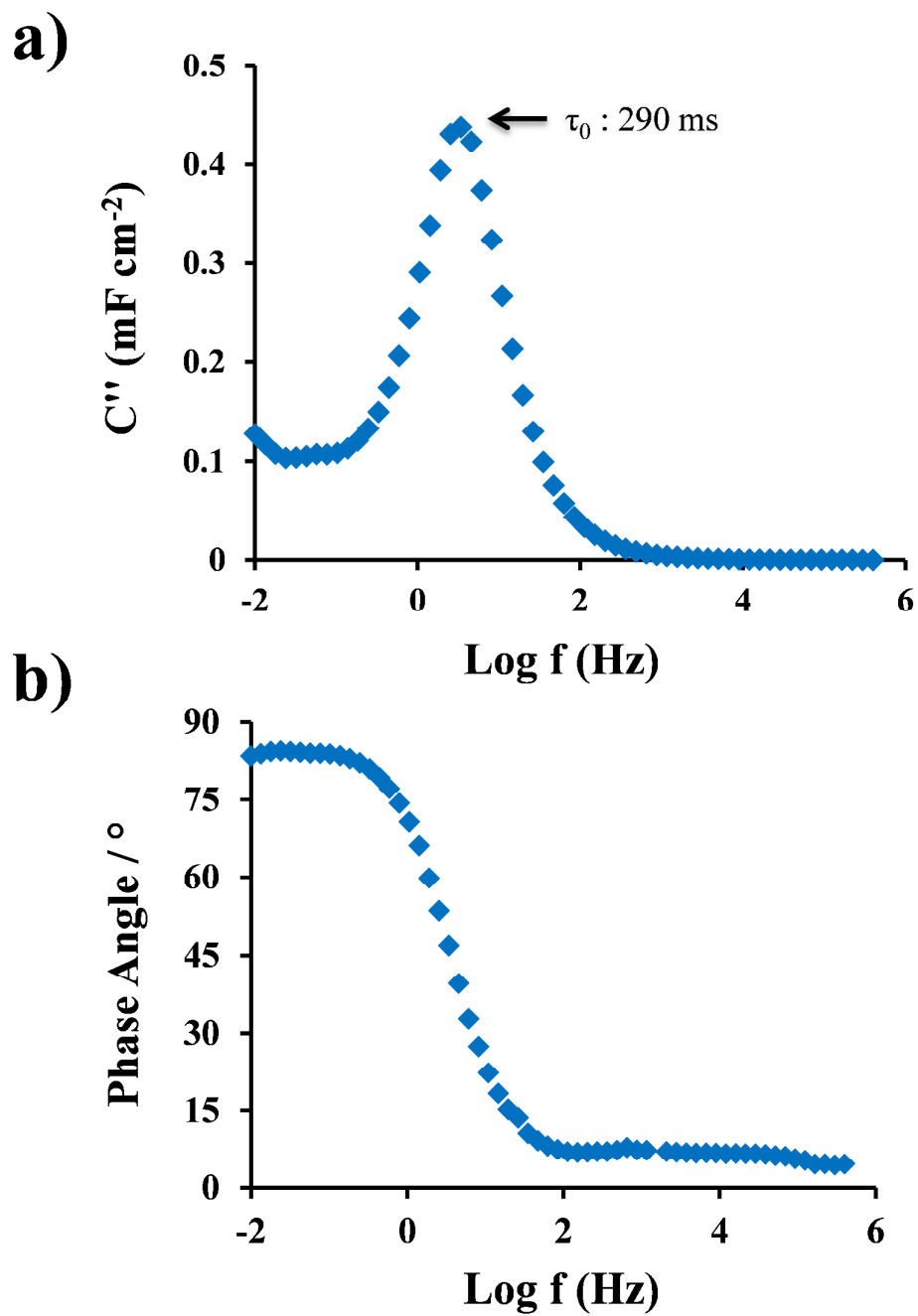


Figure 5

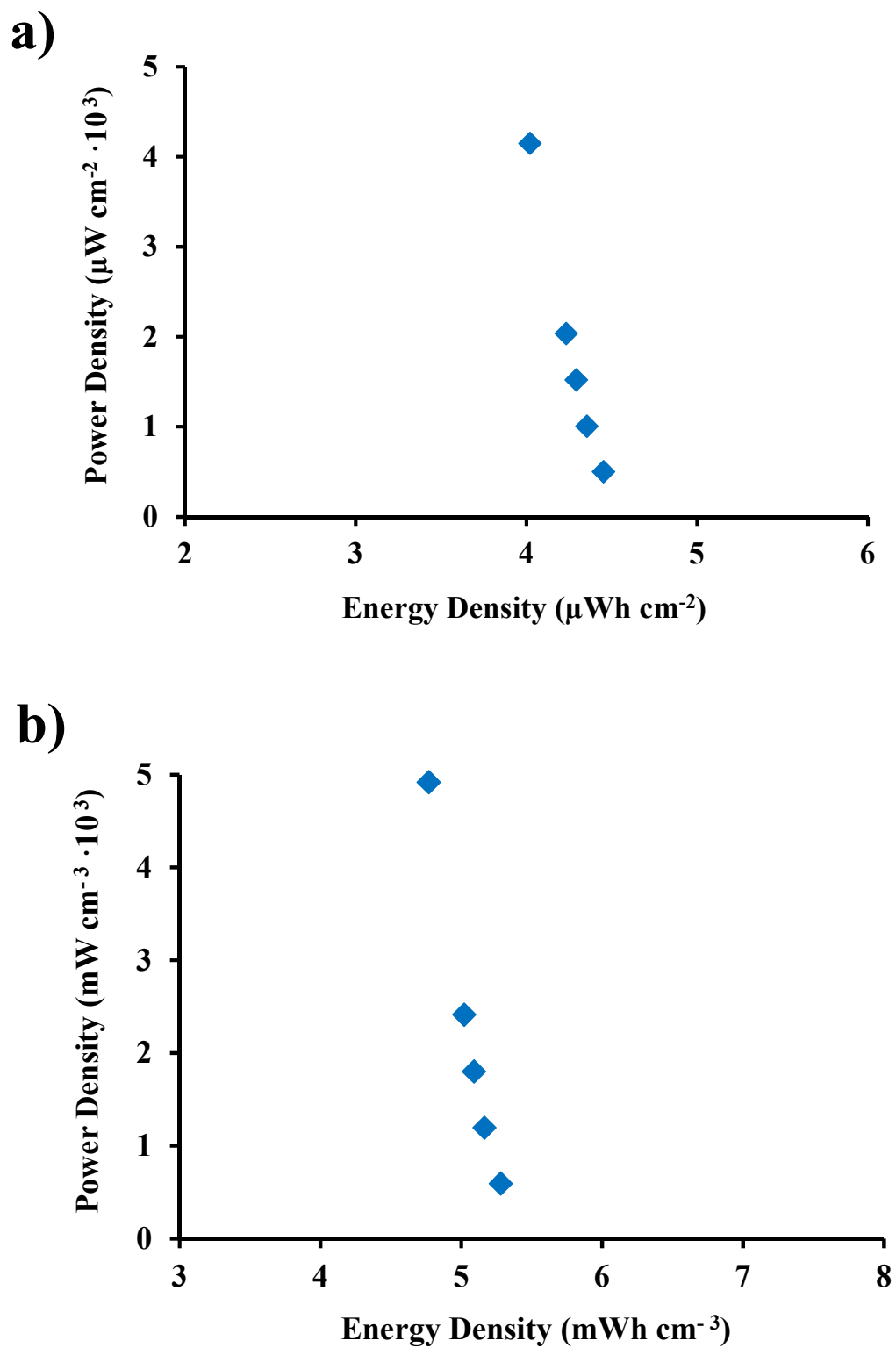


Figure 6

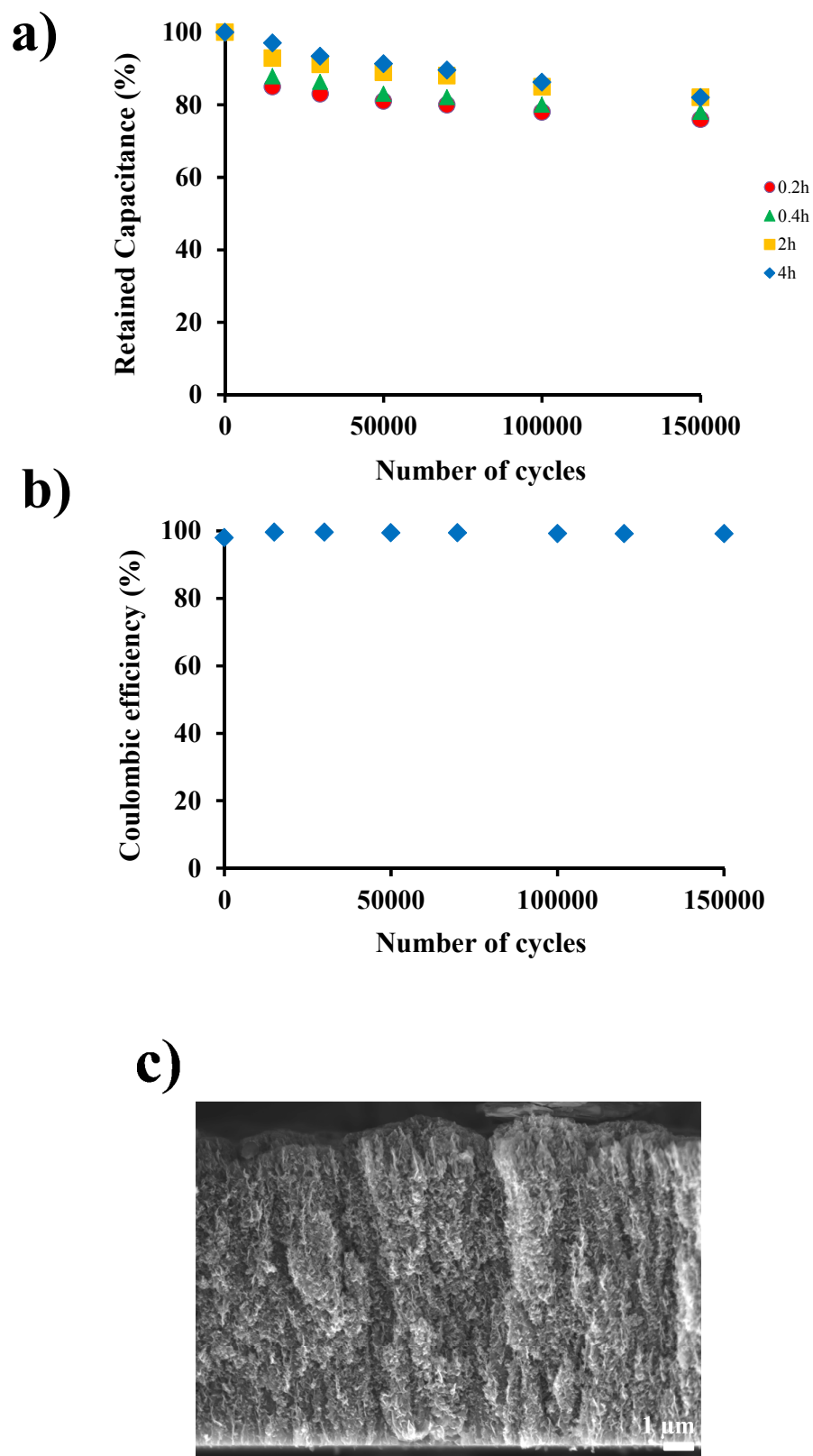
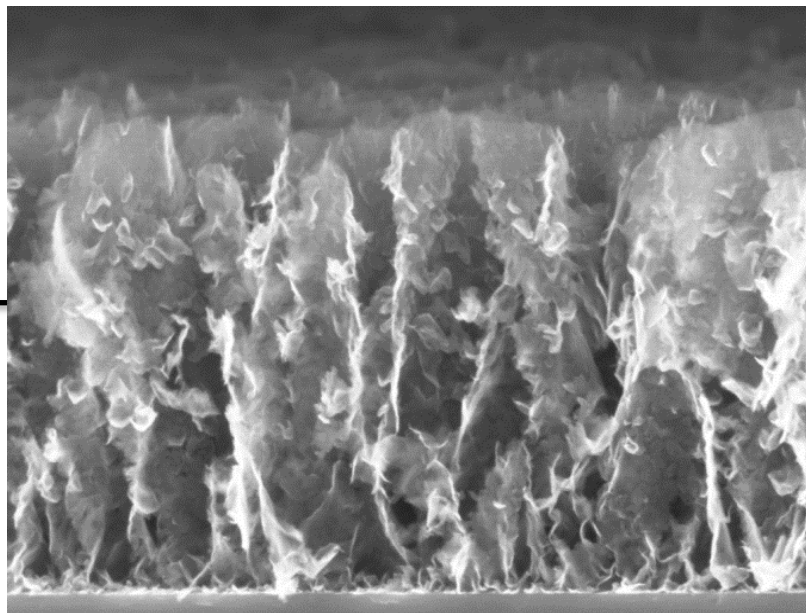


Figure 7



Vertically graphene nanosheets (VGNs)

